# Photo-induced charge state conversion of $Eu^{2+}$ in $Ca_2ZnSi_2O_7$

Hayato Kamioka,[1,a)] Masahiro Hirano,[2] and Hideo Hosono[3]
[1]*Graduate School of Pure and Applied Sciences, University of Tsukuba, Ten-noudai 1-1-1, Tsukuba, Ibaraki 305-8571, Japan*
[2]*Transparent Electro-Active Materials Project, ERATO-SORST, Japan Science and Technology, Bldg. S2-6F East, Tokyo Institute of Technology, 4259 Nagatsuta, Midori-ku, Yokohama 226-8503, Japan*
[3]*Materials and Structures Laboratory, Tokyo Institute of Technology, 4259 Nagatsuta, Midori-ku, Yokohama 226-8503, Japan*

(Received 29 May 2009; accepted 5 August 2009; published online 8 September 2009)

$Eu^{2+}$ doped sorosilicate $Ca_2ZnSi_2O_7$ (melilite) exhibits a broad band emission peaking at ~600 nm (~2 eV) due to the electric dipole allowed transition of $4f^6 5d^1$ to $4f^7$ of $Eu^{2+}$ by an excitation with blue light (460 nm). Strong $O^{2-}$ ligand field with low symmetry due to the layered tetragonal crystallographic structure of the melilite may play a dominant role in lowering the emission band energy to ~2 eV. In addition, line emissions attributable to the transitions from $^5D_0$ to $^7F_J$ of $Eu^{3+}$ ions are detected by an excitation with deep UV light with sub-360 nm wavelengths. This is due to the formation of transient $Eu^{3+}$ ions via charge transfer from $Eu^{2+}$ to the matrix. The lifetime of the transient $Eu^{3+}$ ion is found to be 58 ms by a pump-probe measurement, in which UV pulse laser and green continuous wave laser are employed as pump and probe lights, respectively. Based on these results, the energy diagram of $Eu^{2+}$ in $Ca_2ZnSi_2O_7$ is proposed. © *2009 American Institute of Physics*. [doi:10.1063/1.3213360]

## I. INTRODUCTION

Both divalent and trivalent Eu ions in solids exhibit efficient emissions and they have been used widely in commercial phosphors although their optical characteristics differ greatly from each other. That is, the emission and absorption spectra of $Eu^{3+}$ ions are characterized by sharp lines due to $4f^6 \leftrightarrow 4f^6$ ($f$-$f$) transitions. They have been studied extensively, encouraged by applications to red phosphors for fluorescent lamps and color television screens. Their energies are almost insensitive to environments around the ions because $4f$ electrons are electrostatically shielded by other outer electrons. In addition, the $f$-$f$ transition probability is small because it is prohibited by the parity preservation rule, which becomes partially allowed by the spin-orbit interaction and/or odd components of the crystal field. On the other hand, $Eu^{2+}$ ions exhibit broad absorptions and emissions, originating from $4f^7 \leftrightarrow 4f^6 5d^1$ ($f$-$d$) electric dipole allowed transitions. These ions are used in phosphors and scintillator materials for various wavelengths because the energy positions of the $5d$ levels depend strongly on the crystalline environment. Thus phosphors activated with the $Eu^{2+}$ ions can potentially be used for emitting colors from blue to red.[1] Long wavelength emissions of up to 600 nm have been achieved through a rational selection of matrices based on the following three factors. First, there is orbital overlapping between $Eu^{2+}$ and surrounding anions. It lowers the barycentric energy position of the $5d$ level compared to the free ion through the attenuation of the Coulomb repulsion between them, known as the nephelauxetic effect. Second, there is crystal field splitting, in which the degeneracy of the $5d$ state of $Eu^{2+}$ is lifted by the crystal field. The magnitude of the splitting depends on the distances between the $Eu^{2+}$ and ligand ions as well as ligand configurations. The splitting leads to the energy lowering of the $5d$ emitting level, while keeping the barycentric energy unchanged. Finally, electron-phonon interaction contributes to the lowering of the emission band energy, known as a Stokes shift. Here transition energy is partly used to excite phonons through lattice relaxation around the $Eu^{2+}$ site. With an increase in cage size or softening in the cage configuration, the redshift of the emission becomes enhanced.

Recent efforts in exploring $Eu^{2+}$-activated phosphors have been focused on obtaining emission peaking around 600 nm. One may obtain white light-emitting diodes (LEDs) by combining the $Eu^{2+}$ emission with blue light from diodes used as excitation sources. Several phosphors emitting long wavelength light have already been reported, including $Ba_3SiO_5$ (590 nm),[2] $Sr_2SiO_4$ (555 nm),[3] and $Ba_2Mg(BO_3)_2$ (608 nm),[4] in which the $Eu^{2+}$ sites are commonly surrounded by six to nine oxygen ions in a tight configuration, i.e., a strong ligand field. In sorosilicate $Ca_2ZnSi_2O_7$ (melilite), the $Eu^{2+}$ ion, occupies a $Ca^{2+}$ site, is coordinated with eight oxygen, which is comparable to that in these phosphors. Moreover, the ligand configuration may be tighter because of the layered structure of the melilite. For instance, the average distance between nearest coordinated ligand oxygen and $Eu^{2+}$ in $Ca_2ZnSi_2O_7$ (2.6 Å) is much smaller than that in $Ba_2Mg(BO_3)_2$ (2.812 Å),[4] $Ba_3SiO_5$ (2.856 Å),[5] and $Sr_2SiO_4$ (2.702 Å).[6] Therefore, one may expect that $Eu^{2+}$ doped sorosilicate $Ca_2ZnSi_2O_7$ would emit longer wavelength light even compared with these phosphors.

The valence state of Eu may be changed between $Eu^{2+}$ and $Eu^{3+}$ with a high-energy photon. In fact, several efforts have been made in applying this process to optical storage devices and detection of high-energy irradiation. This process has been suggested in $Sr_2SiO_4$:$Eu^{3+}$ under UV light or

a)Electronic mail: kamioka@sakura.cc.tsukuba.ac.jp.

 

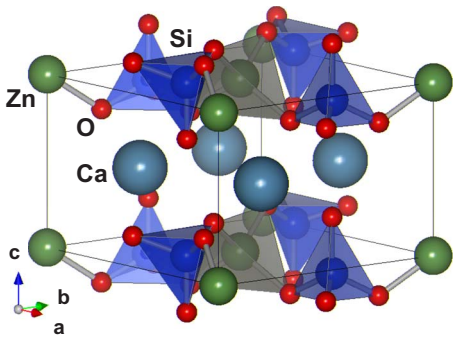


FIG. 1. (Color online) Crystal structure of $Ca_2ZnSi_2O_7$.

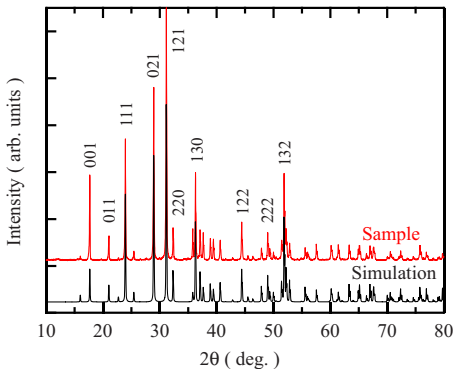


FIG. 2. (Color online) XRD patterns of $Eu^{2+}$ doped $Ca_2ZnSi_2O_7$.

x-ray irradiation,[2] where a sharp-line emission spectrum became broad band emission due to $Eu^{3+}$ being photoreduced to $Eu^{2+}$. The reverse process has also been proposed in $Y_2O_2S:Eu^{2+}$ (Ref. 7) and it has been confirmed experimentally in $Sm^{2+}$ doped $SrB_4O_7$ (Ref. 8) and borate glass.[9] Here the divalent $Sm^{2+}$ ion is oxidized and releases an electron. Since this released electron is likely transferred to the conduction band of the host material, or else an electron in the valence band is transferred to $Eu^{3+}$ in the photoreduced process, the ground state energy of $Eu^{2+}$ (or $Eu^{3+}$) relative to the valence and conduction bands of the host is the governing factor in determining whether the Eu valence conversion occurs.

We synthesized single-phase crystals of $Ca_2ZnSi_2O_7:Eu^{2+}$ and measured the photoluminescence (PL), photoluminescence excitation (PLE), and optical absorption (OA) spectra. A broad emission band was observed, peaking at 600 nm, with an excitation wavelength above 360 nm, which is one of the longest emission wavelengths among $Eu^{2+}$-activated oxide phosphors. In addition, the emission spectra exhibit transient sharp lines under UV irradiation (<360 nm), superposed on a broad band, indicating that $Eu^{3+}$ is photogenerated by the UV light irradiation. The results have been reported briefly in our previous report.[10] In this paper, we report experimental results more thoroughly and detailed analysis of the time evolution for the emission due to photoinduced $Eu^{3+}$, which provides direct evidence for the existence of the transient $Eu^{3+}$. Moreover, we have proposed an energy diagram of $Eu^{2+}$ in the host material based on the emission, excitation, and diffused reflection spectra.

## II. EXPERIMENTAL PROCEDURE

### A. Crystal structure and sample preparation

$Ca_2ZnSi_2O_7$ is a member of the melilite group with the tetragonal space group $P\bar{4}2_1m(D^3_{2d})$ [Fig. 1 (Ref. 11)]. The crystal has a layered structure, where each layer is constructed by either corner-shared $[ZnO_4]$ or $[SiO_4]$ tetrahedrons held together, with an additional Ca interlayer inserted in between. The $Ca^{2+}$ site is thus surrounded by eight oxygen ions, which function as ligands. Each four of them belong to distorted cubes in the upper and lower planes and are rotated by 45° with respect to each other. The doped $Eu^{2+}$ ions most likely replace the $Ca^{2+}$ sites because of the charge and ion radius similarity (1.12 Å for $Ca^{2+}$ and 1.25 Å for $Eu^{2+}$).[12]

Stoichiometric mixture of $CaCO_3$, ZnO, and $SiO_2$ powders was blended in ethanol. After desiccation, they were sintered in air at 1300 °C for 6 h. They were then mixed with additional ZnO, $SiO_2$, and $EuCl_3$ powders in acetone and desiccated again. Finally, a pressed pellet was put in a graphite crucible and annealed at 1300 °C in a reduced atmosphere of $H_2:N_2=5:95$ to obtain the phosphor. The valence state of Eu ($Eu^{2+}$) was confirmed from the broad band feature of the PL spectrum. The crystalline phases of the samples were identified by x-ray diffraction (XRD) using a Rigaku RINT 2000 with Cu $K\alpha$ radiation. A typical XRD pattern of a synthesized sample is shown in Fig. 2, together with the simulation pattern obtained from the Inorganic Crystal Structure Database. All of the peaks of the sample were indexed to those of $Ca_2ZnSi_2O_7$, indicating that the samples are composed of a single phase.

### B. Optical measurements

PL and PLE spectra excited by continuous wave (cw) light with excitation wavelengths of 260, 320, 360, 420, and 460 nm were recorded by a fluorescence spectrophotometer (Hitachi F4500). PLE spectra were obtained using a monochromic cw light by monitoring a fixed wavelength of 600 nm, which corresponded to the emission band peak. Spectral diffuse reflection was measured by an UV-visible-near-infrared multipurpose spectrophotometer (Hitachi U4000) with a cw light from a $Xe+D_2$ lamp, which was converted to an OA spectrum via the Kubelka–Munk transformation. Time-resolved PL spectra were taken using nanosecond light pulses (230–540 nm) from an optical parametric oscillator (OPO) pumped by a $Q$-switched neodymium doped yttrium aluminum garnet (Nd:YAG) laser (Spectra-Physics MOPO-SL and PRO290), or femtosecond pulses (at 266 nm) from a third harmonic of a regenerative amplified Ti:sapphire laser (Spectra-Physics Spitfire), and a spectrometer with a streak camera (Hamamatsu-Photonics C5680) at temperatures between 77 and 298 K. The time decay of the PL spectra was measured by a spectrometer equipped with a gated charge coupled device detector (Roper-Scientific SpectraPro500i). Pump and probe measurements were performed using a second harmonic (532 nm) of a Nd:YAG laser (Spectra-Physics Millennia V) as a probe and an UV nanosecond pulse as a pump.

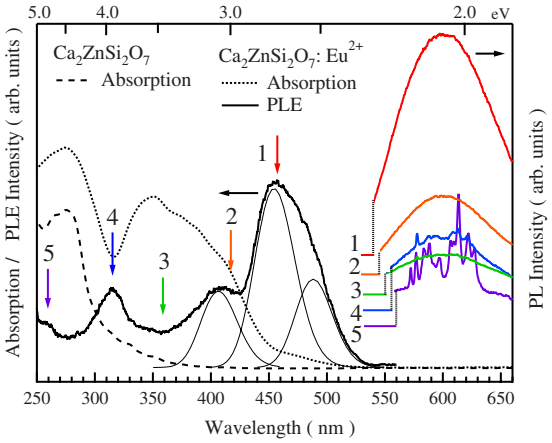


FIG. 3. (Color online) PLE and PL spectra of $Ca_2ZnSi_2O_7$:$Eu^{2+}$ phosphor. The PL spectra were taken at the excitation wavelength between 260 and 460 nm. Emission was monitored at 600 nm for the PLE spectrum. Here, the lowest energy band in the PLE spectrum is decomposed into three Gaussian components. Dotted and dashed lines show the absorption spectrum for the phosphor and the pure matrix, respectively.

## III. RESULTS AND DISCUSSION

### A. cw measurements

Figure 3 shows PL, PLE, and OA spectra for 1% $Eu^{2+}$ doped $Ca_2ZnSi_2O_7$ sample, which gave the most intense PL as a function of $Eu^{2+}$ concentration. Strong PLE bands (at wavelengths of 460 nm, for instance) appear in the weak OA region and vice versa. In an extreme case, dip structures are observed at OA band peak positions of 280 and 360 nm. Such discrepancy is likely due to an "inner-filter effect," which is generally observed in sintered powder phosphors with intense absorption bands. That is, the excitation light corresponding to strong absorption peaks is absorbed mostly on the surface to excite $Eu^{2+}$, which then decays nonradiatively via faintly emitting photons. However, photons that originate away from the peak penetrate deep inside the sample and form excited states uniformly in the bulk. These contribute efficiently to the emission intensity. As a result, the PLE spectrum exhibits the dip structures at wavelengths around OA band peaks.

Comparison between the PLE and OA spectra indicates that the fundamental absorption edge for $Ca_2ZnSi_2O_7$ is located at approximately 280 nm. This is the transition from the valence band, which is dominantly composed of $O_{2p}$, to the conduction band formed by metal orbitals. On the one hand, PL spectra taken with the excitation wavelengths above 360 nm (spectra 1 and 2) show a single emission band peaking at about 600 nm, which is attributable to the *f-d* transition of the $Eu^{2+}$ ion. The peak wavelength is much longer than those observed in most of oxides and fluorides (350–500 nm) and nearly equal to those of Ca-$\alpha$-SiAlON (600 nm) (Refs. 13 and 14) and alkaline-earth chalcogenides (SrS 616 nm, CaS 651 nm).[15] On the other hand, PL spectra excited below 360 nm are composed of sharp lines superposed on the broad band. The emission wavelengths agree with those associated with the intra-4*f* transitions of $Eu^{3+}$ [$^5D_0 \rightarrow {}^7F_J(J=0,1,2,\ldots)$], confirming the assignment of the optical bands at 360 nm in the OA and PLE spectra to charge-transfer absorption from $Eu^{2+}$ to the conduction band. That is, the $Eu^{3+}$ ion is generated as a result of photoreduction of $Eu^{2+}$ to release an electron to the conduction band, which may be captured in electron traps in the conduction band. Thus, the $Eu^{3+}$ ion has a finite lifetime following UV irradiation, as discussed in Sec. III B.

TABLE I. The lattice constants and bond length between alkaline-earth metal (Ca, Sr) and oxygen (Refs. 16–19) for some melilites are listed in angstroms. The corresponding PL peak wavelength and Stokes shift energies are also shown (Ref. 20). Oxygen 1–4 and 5–8 form cubes in the upper and the lower ligand planes, respectively.

| | *M* | | |
|---|---|---|---|
| Ca, Sr | $Ca_2ZnSi_2O_7$ | $Ca_2MgSi_2O_7$ | $Sr_2MgSi_2O_7$ |
| *a* | 7.828 | 7.838 | 7.996 |
| *b* | 7.828 | 7.835 | 7.996 |
| *c* | 5.014 | 5.009 | 5.152 |
| $M-O_1$ | 2.412 | 2.414 | 2.555 |
| $M-O_2$ | 2.412 | 2.414 | 2.555 |
| $M-O_3$ | 2.699 | 2.704 | 2.742 |
| $M-O_4$ | 2.699 | 2.704 | 2.742 |
| $M-O_5$ | 2.472 | 2.469 | 2.565 |
| $M-O_6$ | 2.484 | 2.480 | 2.590 |
| $M-O_7$ | 2.685 | 2.707 | 2.776 |
| $M-O_8$ | 2.685 | 2.707 | 2.776 |
| Average | 2.566 | 2.575 | 2.663 |
| PL | 600 nm | 535 nm | 470 nm |
| S. shift | 630 meV | 760 meV | 670 meV |

Table I summarizes the cation-anion distances for three kinds of melilite compounds estimated from XRD data,[16–19] together with PL wavelengths and magnitudes of the Stokes shifts.[20] Bond distances except those for $-O_4$ and $-O_5$ decrease with a replacement of $Mg^{2+}$ ion by $Zn^{2+}$, in spite of the larger ionic radius of the latter ($Mg^{2+}$=0.89 Å, $Zn^{2+}$=0.90 Å).[12] This discrepancy may be due to a difference in the magnitude of distortion of the tetrahedron, leading to larger shrinkage of the *c*-axis in Zn compound than that in Mg compound. Regardless of the mechanism, the shorter chemical bond lengths in the Zn compound result in the strengthening of the ligand field around the $Eu^{2+}$ site. In addition, a replacement of Ca ion with $Sr^{2+}$ ion may weaken field intensity because of an expanded ligand configuration reflecting their ion radii ($Ca^{2+}$=1.12 Å, $Sr^{2+}$=1.26 Å).[12] Moreover, a replacement of a $Ca^{2+}$ ion with $Ba^{2+}$ ion induces a change in the crystal structure from tetragonal to monoclinic, leading to an expansion of the anion-cation distances to approximately 2.8 Å.[20] As a result, an emission due to the *d-f* transition of $Eu^{2+}$ in $Ba_2MgSi_2O_7$ appears at 505 nm, which is much shorter than that of the tetragonal melilite. The small bond distances between $Eu^{2+}$ and $O^{2-}$ may also give rise to a large covalency, which likely reduces the barycentric energy position of the 5*d* levels. Table I demonstrates that magnitudes of the Stokes shifts are almost equal for the three compounds, suggesting that the Stokes shifts largely do not contribute to long wavelength emission. Thus it may be

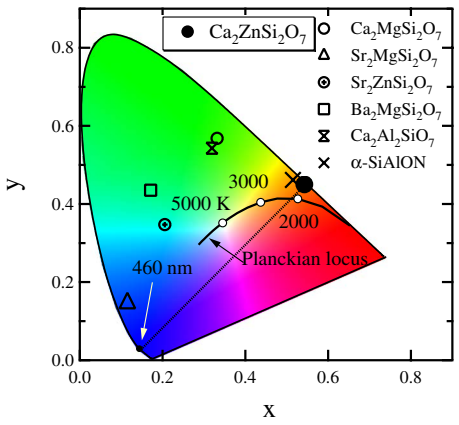


FIG. 4. (Color online) Chromatic coordinates for $Ca_2ZnSi_2O_7:Eu^{2+}$ and several isomorphic compounds. The coordination for Ca-$\alpha$-SiAlON is also plotted as a typical red-orange phosphor.

concluded that the strong ligand field imposed on $Eu^{2+}$ in Ca-melilite plays a critical role in the redshift of the peak wavelength of the emission band.

Existence of a PLE band centered at 460 nm in the PLE spectrum is well suited for excitation by InGaN blue LEDs. Furthermore, the Commission International del'Eclairge (CIE 1931) chromaticity for emission from a 1% Eu-activated $Ca_2ZnSi_2O_7$ is calculated to have an index $(x,y)=(0.542,0.450)$. The chromaticity point, together with those for other melilites, is shown in Fig. 4. It is worth noting that the line connecting the chromaticity points of a blue LED ($\lambda_{em}=460$ nm) and $Ca_2ZnSi_2O_7:Eu^{2+}$ (600 nm) crosses the Planckian locus at color temperatures of ~2000 K. Therefore, the blue LED-excited $Ca_2ZnSi_2O_7:Eu^{2+}$ allows for generating "warm" white light, which had not been realized using commercial $Y_3Al_5O_{12}$ (YAG):Ce phosphor excited with a blue LED.

### B. Time-resolved measurements

To clarify the photoinduced $Eu^{3+}$ state formation, we have performed time-resolved optical measurements since this state is expected to be transient. Streak images for $Ca_2ZnSi_2O_7:Eu^{2+}$ using a 266 nm femtosecond pulse as an excitation light source are shown in Fig. 5. The time-integrated PL spectrum from 0 to 1 ms is plotted as a solid line and reproduces the PL spectra excited by cw light. These emission lines precisely agree with those due to the transitions from the $^5D_0$ emitting state to the $^7F_J$ ground states. The decay profiles of the line emissions were derived from the cross section of the streak images, as seen in Fig. 6. $Ca_2ZnSi_2O_7:Eu$ exhibits broad emission with shorter decay time of about 2.5 $\mu$s, associated with the allowed $d$-$f$ transition of $Eu^{2+}$ ions, followed by line emission with longer decay times of 2.5 ms, which is attributed to the forbidden intra-4$f$ transitions of $Eu^{3+}$ ions. Thus, the PLE spectrum for each component was obtained separately by time-resolved measurements, in which nanosecond pulses underwent tuning in a wide wavelength range.

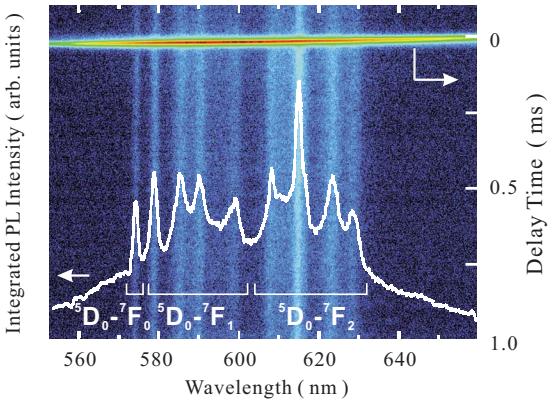


FIG. 5. (Color online) Integrated PL intensity spectrum and contour plot for a streak image with a delay time region of ≤1 ms. The excitation was performed by 266 nm femtosecond pulses at 298 K.

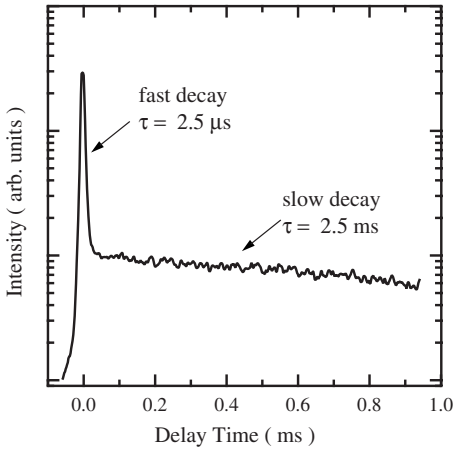


FIG. 6. PL decay profile for the emission line at 617 nm after the excitation with a 266 nm femtosecond pulse at 298 K.

OPO was employed as the excitation light for monitoring emission at 614 nm. The emission at this wavelength is a superposition of a fast $Eu^{2+}$ decay and a slow $Eu^{3+}$ $^5D_0 \rightarrow {}^7F_2$ decay. Figure 7(a) shows a time-integrated PLE spectrum from 0 to 5 $\mu$s for the fast decay component, denoted by filled circles, and from 20 to 80 $\mu$s for the slow decay component, denoted by open squares. cw-light excited PLE is also plotted in the figure by a solid line and resembles the PLE spectra for the fast decay components. However, PLE for the slow component is similar to PLE for $Eu^{3+}$ activated Ca-melilite, which did not undergo a reduction treatment [Fig. 7(b)]. This confirms that the fast and slow components in the time-resolved PLE spectra are due to $Eu^{2+}$ and $Eu^{3+}$, respectively. The PLE spectra for $Eu^{3+}$ suggest that the observed strong band below 300 nm is attributable to the charge-transfer transition, in which an electron in the valence band is transferred to $Eu^{3+}$ to form $Eu^{2+}$ and a hole in the valence band. In addition, the long lifetime of PLE peaks at 395, 465, and 530 nm implies that some $Eu^{3+}$ ions remained in the reduction-treated samples. That is, the dominant portion of the line emission is due to the photogenerated $Eu^{3+}$, although there is a small contribution due to the residual $Eu^{3+}$ ions.

In order to distinguish the contributions due to the photoinduced $Eu^{3+}$ ions from the residual ones, we performed pump-probe measurements to estimate the lifetime of the transient $Eu^{3+}$ ions. Here the samples were irradiated

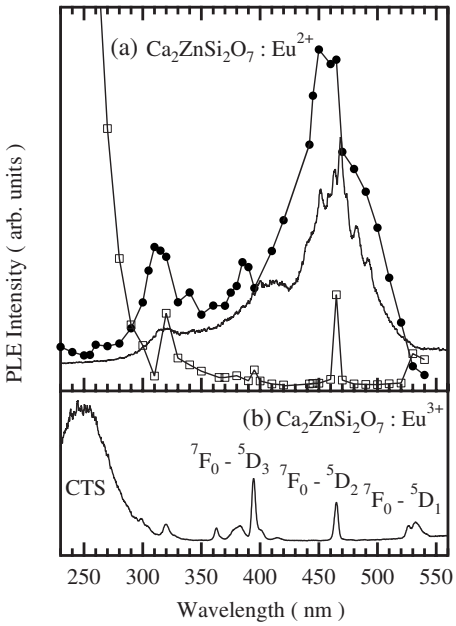


FIG. 7. (a) The time-integrated PLE spectrum for fast (filled circle) and slow (open square) components. cw-measured PLE spectrum is also shown by solid line for comparison. (b) The PLE spectrum for prereduced $Ca_2ZnSi_2O_7$ doped with $Eu^{3+}$ ions.

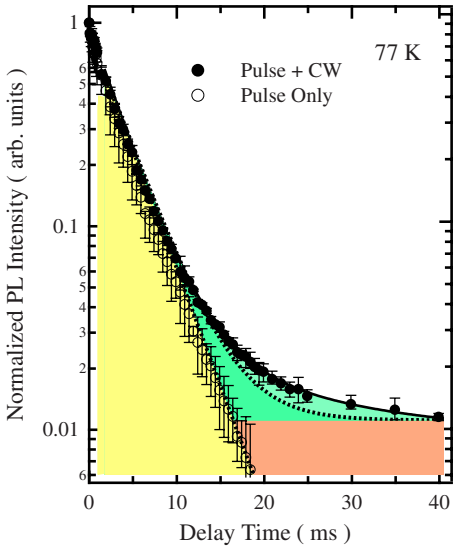


FIG. 9. (Color online) PL decay profiles monitored at 584 nm with a 260 nm excitation. The experimental data were plotted with its error bars. The dotted and solid lines show a fitting curve using single and double exponential functions for the data, respectively. The yellow area is due to $Eu^{3+}$, which were observed without additional 532 nm excitation. Green and brown areas are, respectively, due to the transient $Eu^{3+}$ and residual $Eu^{3+}$ observed with 532 nm excitation.

simultaneously with a nanosecond UV (260 nm) pulse as a pump and green (532 nm) cw laser as a probe, whose energy exactly matched the transition energy from $^7F_0$ to $^5D_1$ states of the $Eu^{3+}$ ions. Figure 8 shows the transitional emission spectra at 77 K for simultaneous irradiation with two kinds of laser light. All the spectra show similar profiles, independent of the time delay from the pulse and are thus assigned to $Eu^{3+}$. The emission intensity was nearly exhausted within ~40 ms, showing that most of the $Eu^{3+}$ ions were transient. Time decay curves of the emission intensity at 584 nm corresponding to $^5D_0 \rightarrow {}^7F_1$ of $Eu^{3+}$ are shown in Fig. 9, with the emission intensity normalized at $t=0$.

The decay from pulse excitation only (open circles in Fig. 9) was fitted well by a single exponential function with a decay time of 3.8 ms (dotted line in Fig. 9). In contrast, the decay curves excited by the pulse and cw light (filled circles in Fig. 9) could not be fitted by a single exponential. Furthermore, a time-independent component (orange area in Fig. 9) was also observed. It persisted for more than 40 ms and indicated that unreduced $Eu^{3+}$ ions still remained in the sample with the photoinduced transient $Eu^{3+}$ ions.

Employing a three-level model (Fig. 10) yields emission rate equations (1) and (2) during the cw-light excitation just after the UV pulse. Here $N_1$, $NN_2$, and $N_3$ are electron densities of $Eu^{2+}$ ground state, $Eu^{3+}$ ground states ($^7F_0$), and $Eu^{3+}$ excited state ($^5D_0$), respectively. Absorption rate from $N_2$ to $N_3$ is given by $\delta$, while $\beta$ represents the emission rate from $N_3$ to $N_2$. The recovery rate of $Eu^{3+}$ to $Eu^{2+}$ is given by $\gamma$. In other words, the lifetime of the transient $Eu^{3+}$ state is given by $1/\gamma$.

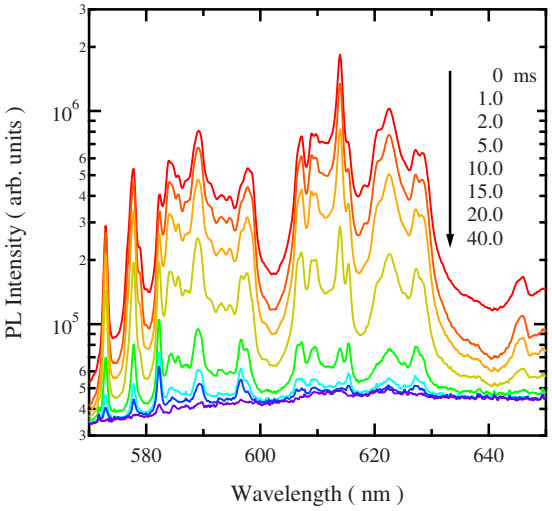


FIG. 8. (Color online) Transient PL spectra obtained with pulse laser excitation at 260 nm.

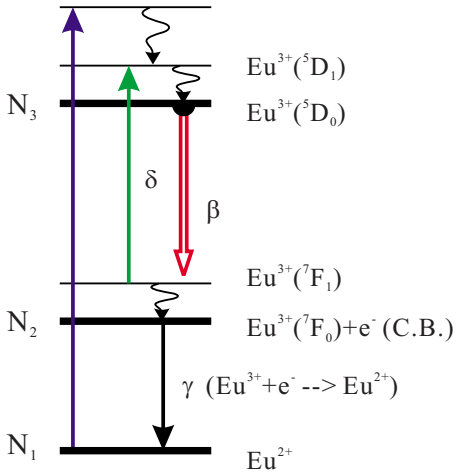


FIG. 10. (Color online) A three-level model for transiently formed $Eu^{3+}$ ion in $Ca_2ZnSi_2O_7:Eu^{2+}$ after 260 nm excitation.

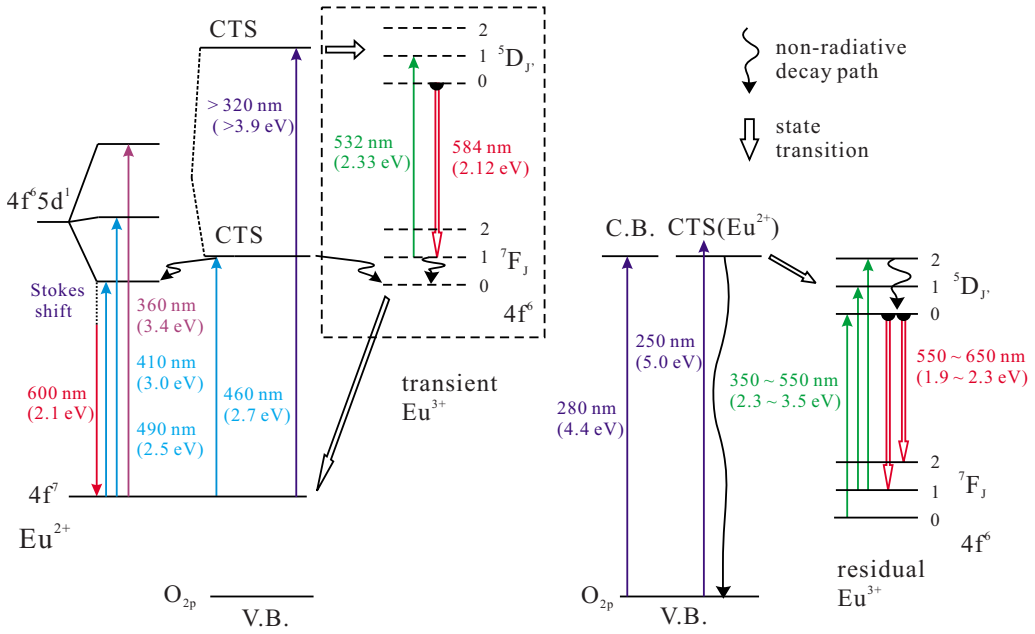


FIG. 11. (Color online) Energy diagram of $Ca_2ZnSi_2O_7$:Eu.

$$\frac{dN_3}{dt} = -\beta N_3 + \delta N_2, \tag{1}$$

$$\frac{dN_2}{dt} = -\delta N_2 + \beta N_3 - \gamma N_2. \tag{2}$$

From this, $N_3$ and $N_2$ are obtained as in Eqs. (3) and (4) below, where $t=0$ is set at the termination of the excitation pulse.

$$N_3 = A_1 e^{-t/\tau_1} + A_2 e^{-t/\tau_2}, \tag{3}$$

$$N_2 = B_1 e^{-t/\tau_1} + B_2 e^{-t/\tau_2}. \tag{4}$$

Here $A_{1,2}$ and $B_{1,2}$ are constants, which depend on the initial conditions, and $1/\tau_{1,2} = -(\beta+\gamma+\delta)/2[1 \pm \sqrt{1-4\beta\gamma/(\beta+\gamma+\delta)^2}]$. Since emission intensity is proportional to $N_3$, Eq. (3) indicates that emission decay follows a double exponential curve, in agreement with experimental observation (solid line in Fig. 9). By fitting Eq. (3) to the experimental curve, the parameters $\tau_1$ and $\tau_2$ are obtained as 14.8 and 3.4 ms, respectively.

When $Eu^{2+}$ is excited by the 260 nm pulse light only, both the excited states $Eu^{2+}$ and $Eu^{3+}$ are generated, with slight amounts of the $Eu^{3+}$ ground state forming at the termination of the pulse. That is, $\delta=0$ in Eq. (1), which leads to a single exponential decay curve ($\tau=1/\beta=3.8$ ms) for the emission from $^5D_0$ of $Eu^{3+}$, in good agreement with the observed decay curve (open circles in Fig. 9). The constant emission intensity after the decay time of 40 ms indicates that there is residual $Eu^{3+}$, which remains unreduced from $Eu^{2+}$ by the reduction treatment. The amount of the residual $Eu^{3+}$ is much smaller than that of the reduced $Eu^{2+}$. As the result of the experiments, the lifetime of the transient $Eu^{3+}(=1/\gamma)$ is estimated to be 58 ms.[21]

We therefore conclude that the $Eu^{2+}$ in $Ca_2ZnSi_2O_7$ photoreleases an electron to form $Eu^{3+}$ when excited by light whose wavelength is shorter than 360 nm. The electron is likely captured at electron traps in the conduction band and may be thermally released over time to recombine with the $Eu^{3+}$, explaining the transient nature of the $Eu^{3+}$ with a lifetime of 58 ms. The emission from the transient $Eu^{3+}$ ions can be induced by sub-360 nm light. In addition, another type of a charge-transfer transition involving $Eu^{3+}$ (electron in the valence band is transferred to $Eu^{3+}$ to form $Eu^{2+}$) is observed at 250 nm in $Ca_2ZnSi_2O_7$ without a reduction treatment.

The most likely energy diagrams of $Eu^{2+}$ (and $Eu^{3+}$) in $Ca_2ZnSi_2O_7$ to explain the observed emission, absorption, and photoexcitation spectra are presented in Fig. 11. Note that the lower energy component of the $4f^65d^1$ states of $Eu^{2+}$ in $Ca_2ZnSi_2O_7$ (emitting states) is supposed to be the tail of the charge-transfer band from the ground state of $Eu^{2+}$ to the conduction band.

## IV. CONCLUSION

We have created a red-orange light-emitting phosphor with blue-light excitation by doping $Eu^{2+}$ into a sorosilicate $Ca_2ZnSi_2O_7$ with a layered structure. A blue-light excitation induces intense broad PL centered at ~600 nm at room temperature, attributable to electric dipole transitions from $4f^65f^1$ to $4f^7$ in $Eu^{2+}$ ions. The observed emission with its unusual long wavelength is due to the low symmetry and tight coordination of the surrounding eight oxygen ions in the layered crystal structure. In addition, line emissions are observed for sub-360 nm deep UV excitation. These originate from the transitions between $^5D_0$ and $^7F_J$ of transient $Eu^{3+}$ ions. It follows that the excitation induces charge transfer from $Eu^{2+}$ to the conduction band of the matrix and simultaneous generation of transient $Eu^{3+}$ ions. We performed pump-probe measurements to confirm the existence of transient $Eu^{3+}$ states, in which the sample was excited by an UV

pulse with cw light exactly tuned to the intra-$Eu^{3+}$ transition. The PL decay profiles signified the generation of the transient $Eu^{3+}$ ions with a lifetime of 58 ms.


[1] P. Dorenbos, J. Lumin. **104**, 239 (2003).
[2] M. Yamaga, Y. Masui, S. Sakuta, N. Kodama, and K. Kaminaga, Phys. Rev. B **71**, 205102 (2005).
[3] A. Nag and T. R. N. Kutty, J. Mater. Chem. **14**, 1598 (2004).
[4] A. Akella and D. A. Keszler, Mater. Res. Bull. **30**, 105 (1995).
[5] E. Tillmanns and H. P. Grosse, Acta Crystallogr., Sect. B: Struct. Crystallogr. Cryst. Chem. **34**, 649 (1978).
[6] M. Catti, G. Gazzoni, G. Ivaldi, and G. Zanini, Acta Crystallogr., Sect. B: Struct. Sci. **39**, 674 (1983).
[7] C. W. Struck and W. H. Fonger, Phys. Rev. B **4**, 22 (1971).
[8] E. Malchukova, B. Boizot, G. Petite, and D. Ghaleb, J. Lumin. **111**, 53 (2005).
[9] A. Kurita, T. Kushida, T. Izumitani, and M. Matsukawa, *Spectral Hole-Burning and Luminescence Line-Narrowing, Science and Applications* (Optical Society of America, Washington, DC, 1992), Vol. 22, p. 163.
[10] H. Kamioka, T. Yamaguchi, M. Hirano, T. Kamiya, and H. Hosono, J. Lumin. **122–123**, 339 (2007).
[11] B. E. Warren and O. R. Trautz, Z. Kristallogr. **75**, 525 (1930).
[12] Y. Q. Jia, J. Solid State Chem. **95**, 184 (1991).
[13] R. J. Xie, N. Hirosaki, K. Sakuma, Y. Yamamoto, and M. Mitomo, Appl. Phys. Lett. **84**, 5404 (2004).
[14] K. Sakuma, K. Omichi, N. Kimura, M. Ohashi, D. Tanaka, N. Hirosaki, Y. Yamamoto, R. J. Xie, and T. Suehiro, Opt. Lett. **29**, 2001 (2004).
[15] H. Kasano, K. Megumi, and H. Yamamoto, J. Electrochem. Soc. **131**, 1953 (1984).
[16] S. J. Louisnathan, Z. Kristallogr. **130**, 427 (1969).
[17] K. Kusaka, K. Hagiya, M. Ohmasa, Y. Okano, M. Mukai, K. Iishi, and N. Haga, Phys. Chem. Miner. **28**, 150 (2001).
[18] M. Kimata, Z. Kristallogr. **163**, 295 (1983).
[19] Z. V. Panina, Yu. A. Malinovskii, G. M. Kuz'micheva, and E. V. Zharikov, Crystallogr. Rep. **40**, 593 (1995).
[20] G. Blasse, W. L. Wanmaker, J. W. ter Vrugt, and A. Bril, Philips Res. Rep. **23**, 189 (1968).
[21] * This is the correct value of $\gamma$. The value of 11 ms estimated in the previous report (Ref. 10) is based on an inappropriate assumption for the solution in the differential equations (1) and (2).